

Sagnac interference in Carbon nanotube loops

GIL REFAEL¹, JINSEONG HEO², MARC BOCKRATH²

¹Dept. of Physics, California Institute of Technology, MC 114-36, Pasadena, CA 91125

² Dept. of Applied Physics, California Institute of Technology, MC 114-36, Pasadena, CA 91125

In this paper we study electron interference in nanotube loops. The conductance as a function of the applied voltage is shown to oscillate due to interference between electron beams traversing the loop in two opposite directions, with slightly different velocities. The period of these oscillations with respect to the gate voltage, as well as the temperatures required for the effect to appear, are shown to be much larger than those of the related Fabry-Perot interference. This effect is analogous to the Sagnac effect in light interferometers. We calculate the effect of interactions on the period of the oscillations, and show that even though interactions destroy much of the near-degeneracy of velocities in the symmetric spin channel, the slow interference effects survive.

Transport measurements on single-walled carbon nanotubes have provided many clear demonstrations of quantum strongly correlated phenomena in mesoscopic physics [1]. Particularly exciting examples include Luttinger-liquid behavior [2, 3], and the Fabry-Perot interference [4, 5] of electrons. These effects, in principle, allow the determination of the interaction parameters of the Luttinger liquid. Nevertheless, previous calculations showed only interference between spin and charge modes with energy scales that were of the same order of magnitude, making experimental observation challenging. In this paper, we propose, analyze, and show initial observations of a new mode of interference - Sagnac interference between two time-reversed paths [6]- in nanotubes forming a loop (i.e. a nanoloop), and with Fermi-surface away from the particle-hole symmetric points. This effect produces large-period fluctuations of the conductance as a function of gate-voltage, and source-drain voltage. Due to its large expected period, this fluctuation effect is expected to survive to very high temperatures.

The Sagnac interferometer measures the angular velocity of a ring, by measuring interference fringes between light propagating inside the ring in two opposite directions. Here we consider the Sagnac effect in an armchair nanotube with a loop (Fig. 1), i.e., two points along the nanotube between which electrons can tunnel (such tunneling effects were discussed in Ref. 7, 8). Electrons impinging on point X in Fig. 1, can either proceed and traverse the loop in a counter-clock-wise direction, or tunnel to point X' , and traverse the loop in a clockwise direction, reproducing the Sagnac interference effect (Fig. 2b). Note that unlike Fabry-Perot interference, in which the interfering beams traverse a different physical distance (e.g. the loop a different number of times) the Sagnac interference is between two beams traversing *exactly* the same distance.

The role of the angular velocity for the light interferometer is replaced with a velocity difference for the two counter propagating electronic beams (Fig. 2b). Using a gate voltage V_g , the Fermi-surface is tuned away from the band middle; ignoring interactions, right and

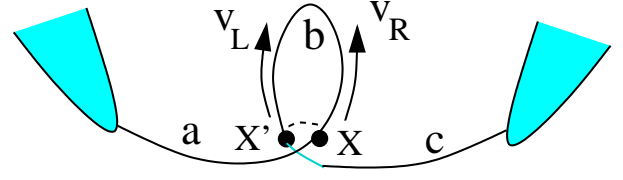


FIG. 1: The system of interest is a nanotube that forms a loop. At the basis of the loop electrons can tunnel (dashed line) from one branch (X) to the other (X'). This produces interference between counter-propagating electrons due to the velocity- difference between right and left-moving electrons.

left moving electrons in one node may have different velocities: $v_R = v_F + u$, and $v_L = v_F - u$ (Fig. 2a)[9]. A small velocity difference u , like a small angular velocity in the light Sagnac effect [6], produces a slow fluctuation of the conductance as a function of V_g [10]. The phase difference between the two interfering beams is:

$$\Delta\phi = Lk_L - Lk_R = \frac{L\epsilon_F}{\hbar v_L} - \frac{L\epsilon_F}{\hbar v_R} \approx \alpha e V_g L \frac{2u}{\hbar v_F^2} \quad (1)$$

where L is the length of the loop, and $\epsilon_F = \hbar v_{R/L} k_{R/L}$. Also, $\epsilon_F = \alpha e V_g$, where α is the conversion factor between the gate voltage and change in chemical potential. Interference fringes repeat when $\Delta\phi = 2\pi n$. Since roughly $u \propto V_g$, the n 'th fringe is at $V_g \propto \sqrt{n}$; fringes are more dense as we move away from the middle of the nanotube's band. For non-interacting electrons, the same fringes should appear as a function of a source-drain voltage, V_{sd} . In the armchair-tube nanoloop, beams moving in the same direction around the loop, but in different nodes, also interfere (Fig. 2c). The two beams in this *band-Sagnac* effect differ by the same phase due to the time-reversal symmetry.

The simple analysis above, which ignores interactions, already provides a good picture of the Sagnac effect in nanotubes. Nevertheless, thin single-walled nanotubes are expected to have a Luttinger parameter $g \sim 0.3$ [4]. Interactions change the hydrodynamic velocities in the nanotube dramatically, and may lift the near degeneracy

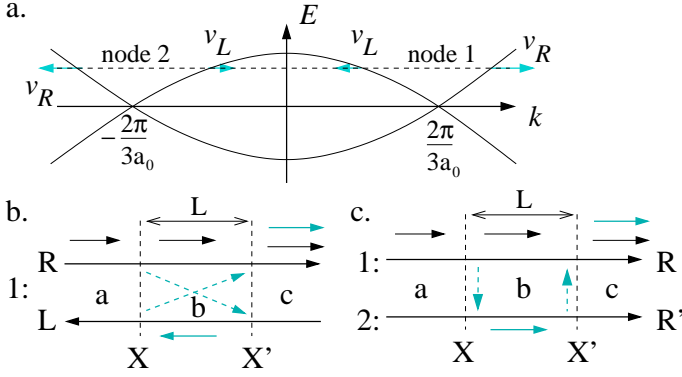


FIG. 2: (a) Dispersion of an armchair nanotube. When the gate voltage is nonzero, the right and left movers in each node have different velocities, $v_{R/L} = v_F \pm u$ (a_0 is the lattice constant). A nonzero $u = (v_R - v_L)/2$ leads to the two Sagnac interference effects: (b) Within one node (say node 1), a beam entering the loop from the left (short black arrow) splits by partially tunneling between points X and X' to two counter-propagating beams (black and gray), in region b. They then recombine at point X'. Long black arrows represent the two chiral electronic modes near node 1. The regions a, b, and c correspond to those indicated in Fig. 1. (c) A beam impinging on point X in node 1 (2) partially scatters to node 2 (1). Both traverse the loop in the same direction (short black and gray arrows), and recombine at point X'. This effect is similar to the slow conductance oscillation due to impurities propounded in Ref. 11, and in the presence of axial magnetic field in Ref. 12.

of the velocities between the interfering beams. In the following we analyze the Sagnac interference effect (and also the Fabry-Perot interference with $u \neq 0$) of interacting electrons. We will show that interactions do not destroy the large-period Sagnac fringes. Yet strong modifications exist: the fringes in the conductance as a function of V_g are determined mostly by the bare, non-interacting, velocity spectrum, essentially reflecting Eq. (1), while the fringes in V_{sd} are modified dramatically, and reflect the four velocities of the tube's hydrodynamic modes.

The bosonized Lagrangian of the two Dirac nodes, with λ parametrizing the density-density interaction, is:

$$\mathcal{L} = \frac{\hbar v_F}{2\pi} \sum_{\sigma, a=1,2} \int dx \left[\frac{2}{v_F} \dot{\theta}_a^\sigma \nabla \phi_a^\sigma - (\nabla \theta_a^\sigma)^2 - (\nabla \phi_a^\sigma)^2 + (-1)^a 2 \frac{u}{v_F} \nabla \phi_a^\sigma \nabla \theta_a^\sigma \right] - \int dx \lambda \left(\sum_{\sigma, a=1,2} \frac{1}{\pi} \nabla \theta_a^\sigma \right)^2. \quad (2)$$

The subscript a designates the Dirac node, σ is the spin. The charge mode, $\frac{1}{2} \sum_{\sigma, a=1,2} (\theta_a^\sigma)$, has the interaction Luttinger parameter $g = (1 + 8\lambda/\pi\hbar v_F)^{-1/2}$. The Fermionic operators are: $\psi_{aR/L}^\sigma \sim e^{i(-1)^a \frac{2\pi}{3a_0} x - i(\phi_a^\sigma \pm \theta_a^\sigma)}$.

The Fourier-transform of (2) defines an 8×8 quadratic form of the θ 's and ϕ 's. Its eight eigenvalues are square-roots of second degree polynomials of ω and k . The dispersion of the eight chiral modes is given by the values of

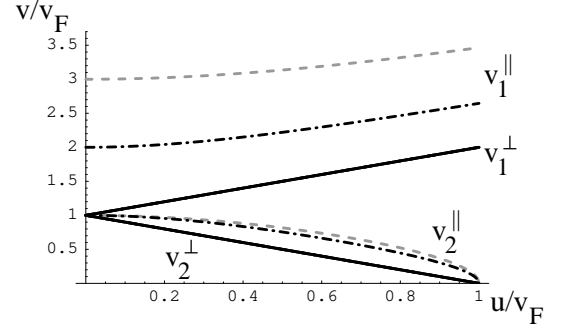


FIG. 3: The velocities of the four hydrodynamic modes as a function of left-right asymmetry of the non-interacting spectrum. Roughly speaking, v_1^{\parallel} corresponds to the charged mode (spin and node symmetric), and v_2^{\parallel} is spin symmetric but node antisymmetric. $v_{1,2}^{\perp}$ are due to the spin-anti-symmetric modes in nodes 1 and 2. The solid line has $g = 1/2$, dashed gray has $g = 1/3$.

ω/k which make an eigenvalue vanish. We find that the spin anti-symmetric channel consists of four untouched neutral chiral modes, with velocities:

$$v_{1\pm}^{\perp} = \pm v_F + u \quad v_{2\pm}^{\perp} = \pm v_F - u \quad (3)$$

where $+$ and $-$ indicate right and left movers respectively. More interestingly, the remaining four spin-symmetric chiral modes are given by (see also Ref. 13):

$$\frac{v_{1,2}^{\parallel}}{v_F} = \frac{1}{\sqrt{2}} \sqrt{1 + \frac{1}{g^2} + 2 \frac{u^2}{v_F^2} \pm \sqrt{\left(1 - \frac{1}{g^2}\right)^2 + 8 \frac{u^2}{v_F^2} \left(1 + \frac{1}{g^2}\right)}} \quad (4)$$

v_1^{\parallel} and v_2^{\parallel} describe two right-left symmetric branches of the spectrum. v_1^{\parallel} is the charge mode velocity, when $u = 0$. The four velocities are depicted in Fig. 3. In the absence of spin scattering, only the spin-symmetric modes can interfere with each other, but the velocities related to these two modes are very different, as can be seen by Eq. (4). In the following, we determine which velocities appear, then, in the interference fringes of V_g and V_{sd} .

V_g couples to the total electronic density, whereas V_{sd} couples to the density difference of right and left movers:

$$\mathcal{L}_{g+sd} = \int dx \left(\alpha e V_g \frac{1}{\pi} \nabla \sum_{\sigma, a} \theta_a^\sigma + e V_{sd} \frac{1}{\pi} \nabla \sum_{\sigma, a} \phi_a^\sigma \right). \quad (5)$$

V_g changes the chemical potential and Fermi-surface of the electrons. This is seen by absorbing the new term in the θ and ϕ gradient terms (where the latter is involved only due to the difference in the original right and left moving velocities). Unlike V_g , V_{sd} drives the system out of equilibrium: it induces a current. This entails a time-dependent transformation of the bosonic fields to absorb

the term. The transformation:

$$\begin{aligned}\tilde{\theta}_a^\sigma &= \theta_a^\sigma - \frac{\alpha g^2 e V_a}{\hbar v_F} \frac{1}{1-g^2 u^2/v_F^2} x + \frac{e V_{sd}}{\hbar} t, \\ \tilde{\phi}_a^\sigma &= \phi_a^\sigma - (-1)^a \frac{\alpha g^2 e V_a}{\hbar v_F} \frac{u/v_F}{1-g^2 u^2/v_F^2} x,\end{aligned}\quad (6)$$

absorbs both V_g and V_{sd} in the bosonic fields, with $\sigma = \uparrow, \downarrow$, and $a = 1, 2$ is the node. The slow, u -dependent, fluctuations can already be noticed in ϕ_a^σ 's x -dependence. The above procedure is drawn from Ref. 5.

Following are the possible scattering processes contributing to transport through the nanoloop. For simplicity, we define $\tilde{\psi}_{aR/L}^\sigma \sim e^{i(-1)^a \frac{2\pi}{3a_0} x - i(\tilde{\phi}_a^\sigma \pm \tilde{\theta}_a^\sigma)}$. The simplest term is the **same-node back-scattering**:

$$\hat{B}(x, t) = b \sum_{\sigma, a} \left(\tilde{\psi}_{aR}^{\sigma\dagger}(x) \tilde{\psi}_{aL}^\sigma(x) e^{2ik_g x - 2i\omega_{sd} t} + \text{h.c.} \right), \quad (7)$$

$$\text{with: } k_g = \frac{\alpha e g^2 V_G}{\hbar v_F (1-g^2 u^2/v_F^2)}, \quad \omega_{sd} = e V_{sd} / \hbar v_F. \quad (8)$$

Second is **cross-node back-scattering**: $\hat{N}_b(x, t) =$

$$n_b \sum_{\sigma, a} \left(\tilde{\psi}_{aR}^{\sigma\dagger}(x) \tilde{\psi}_{\bar{a}L}^\sigma(x) e^{2ik_g \left(1+(-1)^a \frac{u}{v_F}\right) x - 2i\omega_{sd} t} + \text{h.c.} \right), \quad (9)$$

which is backscattering from node a , to node, $\bar{a} = 3 - a$.

Third is **cross-node forward-scattering**: $\hat{N}_f(x, t) =$

$$n_f \sum_{\sigma, a} \left(\tilde{\psi}_{aR}^{\sigma\dagger}(x) \tilde{\psi}_{aR}^\sigma(x) + \tilde{\psi}_{aL}^{\sigma\dagger}(x) \tilde{\psi}_{aL}^\sigma(x) \right) e^{2i(-1)^a \frac{k_g u}{v_F} x}. \quad (10)$$

Most important is the backscattering term arising from tunneling between point X at $x = 0$, and X' at $x = L$ (Fig. 2a) , i.e., **cross-loop back-scattering**:

$$\begin{aligned}\hat{K}_b(t) &= k_b \sum_{\sigma, a, b} \left(\tilde{\psi}_{aR}^{\sigma\dagger}(0) \tilde{\psi}_b^\sigma(L) e^{ik_g \left(1-(-1)^b \frac{u}{v_F}\right) L - 2i\omega_{sd} t} \right. \\ &\quad \left. + \tilde{\psi}_{aL}^{\sigma\dagger}(0) \tilde{\psi}_b^\sigma(L) e^{-ik_g \left(1+(-1)^b \frac{u}{v_F}\right) L + 2i\omega_{sd} t} + \text{h.c.} \right).\end{aligned}\quad (11)$$

To calculate the conductance fluctuations, we must follow the Kubo/Keldysh formalism as it applies to the various scattering events, $\hat{L}_m(x, t)$, where $\hat{L}_m = \hat{B}, \hat{N}_{f/b}, \hat{K}_b$. We defer an exact evaluation to a later publication, and concentrate here on the main features of the fluctuations:

$$\Delta G_{mn} \sim \int_0^\infty dt \langle [\hat{L}_m(t), \hat{L}_n(0)] \rangle \sim \langle \hat{L}_m \hat{L}_n \rangle_{\omega=2eV_{sd}/\hbar}. \quad (12)$$

The second relation, connecting the integral to the correlation's Fourier transform, is due to the time dependence of the integrand being $e^{2i\omega_{sd} t} = e^{2ieV_{sd} t/\hbar}$. In the case of \hat{L}_m occurring at $x = 0$ and \hat{L}_n at $x = L$, the dependence of the oscillating part of ΔG_{mn} on V_{sd} is easily seen to be of the form:

$$\Delta G_{mn} = f \left(e^{2i\omega_{sd} L/v_1^\parallel}, e^{2i\omega_{sd} L/v_2^\parallel}, e^{2i\omega_{sd} L/v_{1+}^\perp}, e^{2i\omega_{sd} L/v_{2+}^\perp} \right), \quad (13)$$

type	$\hat{L}_m \hat{L}_n$	δV_g	T_c
L-SAG	$\hat{K}_b \hat{K}_b$	$\frac{\pi \hbar v_F}{\alpha e g^2 L} \left(1 - \frac{u^2 g^2}{v_F^2} \right) \frac{v_F}{u}$	$\frac{\pi \hbar v_F}{L} \left(1 - \frac{u^2 g^2}{v_F^2} \right) \frac{v_F}{u}$
B-SAG	$\hat{N}_f (\hat{N}_b \hat{B})$	$\frac{\pi \hbar v_F}{\alpha e g^2 L} \left(1 - \frac{u^2 g^2}{v_F^2} \right) \frac{v_F}{u}$	$\frac{\pi \hbar v_F}{L} \left(1 - \frac{u^2 g^2}{v_F^2} \right) \frac{v_F}{u}$
FP	$\hat{B} \hat{B}$	$\frac{\pi \hbar v_F}{\alpha e g^2 L} \left(1 - \frac{u^2 g^2}{v_F^2} \right)$	$\frac{\pi \hbar v_F}{L} \left(1 - \frac{u^2 g^2}{v_F^2} \right)$
B-FP \pm	$\hat{N}_b \hat{N}_b$	$\frac{\pi \hbar v_F^2}{\alpha e g^2 L} \frac{1-u^2 g^2/v_F^2}{v_F^2 \pm u}$	$\frac{\pi \hbar v_F^2}{L} \frac{1-u^2 g^2/v_F^2}{v_F^2 \pm u}$
L-FP \pm	$\hat{K}_b \hat{B}, \hat{K}_b \hat{N}_b$	$\frac{2\pi \hbar v_F^2}{\alpha e g^2 L} \frac{1-u^2 g^2/v_F^2}{v_F \pm u}$	$\frac{2\pi \hbar v_F^2}{L} \frac{1-u^2 g^2/v_F^2}{v_F \pm u}$

TABLE I: Interfering contributions to the conductance as a function of V_g . The first row indicates the type of interference. The loop-Sagnac (L-SAG) and band-Sagnac (B-SAG) correspond to Fig. 2b,c respectively. The three Fabry-Perot modes originate from optical-path difference: of two-loops in node 1 or 2 (B-FP \pm), of one loop in node 1 and one in 2 (FP), or, due to loop-tunneling, one loop in node 1 or 2 (L-FP \pm). The coherence temperature of each interference mode is determined heuristically by assuming that $T_c \sim \alpha g^2 e \delta V_g / k_B$.

where $v_{1/2}^{\parallel/\perp}$ are the four propagation velocities of the various hydrodynamic modes found in Eqs. (4) and (3). Thus we find that the interference fringes as a function of V_{sd} are determined by the velocities of the interaction-induced four hydrodynamic modes.

Our main result is the interference pattern in G vs. V_g . From the various scattering events we infer that only two expressions give rise to interference effects in V_g : $\exp(2ik_g L)$ and $\exp(2ik_g L \frac{u}{v_F})$, with k_g defined in Eq. (8). Table I enumerates the conductance fluctuations due to second-order scattering. Our focus is the loop-Sagnac interference between counter-propagating beams in an interacting nanotube, which is the first line in Table I). Indeed, it coincides with the band-Sagnac interference (B-SAG); it is possible, however, to distinguish the two Sagnac modes by applying a magnetic flux to the loop. The band-Sagnac fringes will be unaffected, whereas the loop-Sagnac phase-difference will be shifted by $2e\Phi/\hbar$, where Φ is the flux through the loop.

A remarkable difference between the Sagnac and Fabry-Perot interference is the sensitivity to temperature. Using a simple argument we estimate the maximum temperature for each interference. The kinetic energy of a single electron has uncertainty of order T . This could be thought of as an uncertainty in the gate voltage: $\Delta V_g \sim T_c / \alpha g^2 e$. When $\Delta V_g \approx \delta V_g$, an interference fringe disappears, which is how we obtain T_c in Table I. A subtle point is the absence of g^2 in the T_c column in Table I; since temperature only smears the kinetic energy of electrons, the effects of interactions should be omitted to first approximation, hence the cancellation of αg^2 . We find that T_c for the Sagnac modes is v_F/u larger than that of the Fabry-Perot interference.

$$T_c^{SAG} \sim \frac{\pi \hbar v_F}{L} \left(1 - \frac{u^2 g^2}{v_F^2} \right) \frac{v_F}{u} \sim \frac{v_F}{u} T_c^{FP} \quad (14)$$

Hence the limiting factor for the observation of the Sagnac effect is most likely phonon scattering.

The experimental observation motivating this work is shown in Fig. 4. At $T = 32K$ fast oscillations with period $\delta V_g \sim 0.3V$ appear; we identify them with the loop-FP mode of Table I (Coulomb blockade is determined by the total wire length, and is expected at a much lower $\delta V_g \sim 10^{-3} - 10^{-2}V$). Another fast mode appears at $T = 12K$, with a doubled frequency, $\delta V_g \sim 0.15V$, and therefore fits the regular FP mode. But in addition, a slowly oscillating envelope of the conductance is already evident at $T = 64K$, with the first period being roughly $\delta V_g \sim 20V$ [14]. If we identify this with the Sagnac effects, then $\delta V_g^{SAG}/\delta V_g^{FP} \sim 130$. To see if this is indeed feasible, we approximate the nanotube's dispersion as parabolic, $\pm\epsilon_k = -\gamma(1 - (\frac{2\pi}{3a_0})^2 k^2)$; and $\frac{u}{v_F} \approx \frac{\epsilon}{2\gamma}$. The first fringe due to the Sagnac interference appears when the accumulated phase difference between the two interfering beams is π :

$$\Delta\phi = \int_0^{\mu^{SAG}} d\epsilon \frac{L}{\hbar v_F} \frac{2u}{v_F} \approx \frac{L}{\hbar v_F} \frac{(\mu^{SAG})^2}{2\gamma} = \pi, \quad (15)$$

where the integral is necessary due to the dependence of u/v_F on ϵ . The first fringe due to Fabry-Perot interference is when $\mu^{FP}2L/\hbar v_F = \pi$. Using $L = 7\mu m$ and $v_F = 8 \cdot 10^5 m/s$, and $\gamma \approx 2.5eV$ [9], we obtain $V_g^{SAG}/V_g^{FP} = \mu^{SAG}/\mu^{FP} \sim 300$, which agrees with the experiment up to a factor of 2. This extra factor might be due to the Fabry-Perot interference arising not from the loop, but from the shorter sections of the nanotube. The experimental results are also consistent with the fact that the Fabry-Perot interference are expected roughly at: $T_c^{FP} \sim \frac{2\pi\hbar v_F}{L} \sim 10K$. Since currently only two samples of the loop geometry are available, we limit ourselves to the order-of-magnitude analysis above, and defer a detailed analysis of the experiment to a future publication.

In addition to the Sagnac interference, we also obtained the modification of the Fabry-Perot interference in the presence of right-left asymmetry and interactions. Most interesting in this respect are the loop- and band-FP effects. In a non-interacting system, these arise from one of the interfering beams going through the loop once, or twice, more than the other, but in a single band. These effects, with a minus sign in Table I, $\delta V_g = \frac{\pi\hbar v_F^2}{\alpha e g^2 L} \frac{1-u^2 g^2/v_F^2}{v_F-u}$, present the *only* interference that may increase their period as V_g tunes away from the Dirac nodes. Slow nanotube conductance oscillations were also seen in Ref. 15, and at first interpreted as Fabry-Perot interference between two closely-spaced localized impurities on the nanotube. Ref. 11, tried to explain them as an impurity interference effect, similar to what we call the band-Sagnac effect (Fig. 2c). But the period of these oscillations increases with distance from the middle of the band, contrary to Ref. 15 observations. Thus we conclude that the slow interference of Ref.[15] may in-

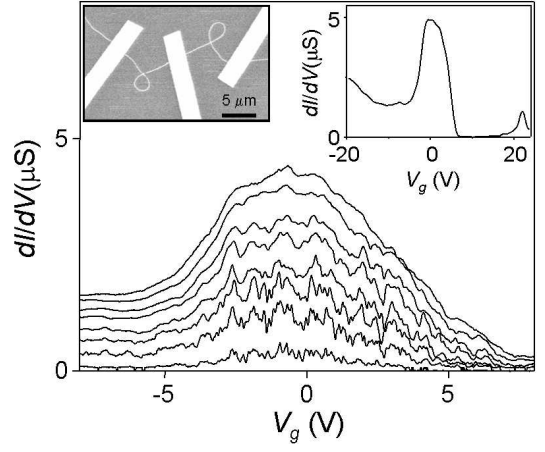


FIG. 4: Conductance vs. gate-voltage of a nanoloop device. From top to bottom: $T = 64K, 48K, 32K, 24K, 16K, 12K, 8K, 4K$. Strong conductance fluctuations appear already at $T = 64K$ with period $\delta V_g \sim 20V$. These fluctuations are consistent with the Sagnac interference effects. At lower temperatures higher-frequency Fabry-Perot interference appears as well with periods $\delta V_g \sim 0.15V, 0.3V$. Left inset shows a scan of the device; data from both loops is qualitatively the same. Right inset shows the suspected Sagnac envelope at $T=4K$ and $V_{sd} = 30mV$ for wider range of V_g . Note that the asymmetry in V_g is not understood.

deed be due to band-Fabry-Perot interference between closely-spaced impurities.

In this paper we discussed the Sagnac and Fabry-Perot interference effects in interacting nanotube loops, with $v_R - v_L = 2u \neq 0$. We found that V_g changes the 'carrier wave' and induces fluctuations that depend mostly on the bare dispersion of the nanotube, while V_{sd} produces fluctuations whose periods depend on the velocities of the non-equilibrium hydrodynamic modes. By studying these conductance fluctuations experimentally, one could in principle extract all hydrodynamic velocities, the interaction parameter, and the bare electron dispersion. We also provided rough estimates of the coherence temperatures, T_c , required to see the Sagnac interference, and showed that it is much higher than that of the Fabry-Perot interference. The estimates of T_c are expected to be modified by a precise inclusion of interactions; this we will pursue in a future publication, in addition to the explicit dependence of the conductivity on V_{sd} . The Sagnac interference is closely related to the interference giving rise to weak localization, therefore its analysis could directly determine the temperature and interaction dependence of the electronic dephasing time τ_ϕ (see further Ref. [16, 17]). Here we showed that the Sagnac effect clearly survive interactions at $T = 0$, therefore our results can be interpreted as evidence for the divergence of τ_ϕ in an interacting electronic system.

We are grateful to J. von Delft and Y. Oreg for a crit-

ical discussion of the manuscript, and to L. Balents, E. Demler, D. Feldman, V. Galitski, and J. Meyer for helpful comments. GR thanks the KITP where part of this work took place. MB and JH are grateful to support by the ONR.

-
- [1] S. J. Tans, M. H. Devoret, R. J. A. Groeneveld, and C. Dekker, *Nature* **394**, 761 (1998).
 - [2] C. Kane, L. Balents, and M. P. A. Fisher, *Phys. Rev. Lett.* **79**, 5086 (1997).
 - [3] M. Bockrath, D. H. Cobden, J. Lu, A. G. Rinzler, R. E. Smalley, L. Balents, and P. L. McEuen, *Nature* **397**, 598 (1999).
 - [4] W. Liang, M. Bockrath, D. Bozovic, J. H. Hafner, M. Tinkham, and H. Park, *Nature* **411**, 665 (2001).
 - [5] C. S. Pea, L. Balents, and K. J. Wiese, *Phys. Rev. B* **68**, 205423 (2003).
 - [6] G. Sagnac, *Comptes Rendus de l'Academie des Sciences (Paris)* **157**, 708 (1913).
 - [7] A. Komnik and R. Egger, *Phys. Rev. Lett.* **80**, 2881 (1998).
 - [8] H. W. C. Postma, M. de Jonge, Z. Yao, and C. Dekker, *Phys. Rev. B* **62**, R10653 (2000).
 - [9] M. Ouyang, J.-L. Huang, and C. M. Lieber, *Phys. Rev. Lett.* **88**, 066804 (2002).
 - [10] Note that another interesting work that relies on $u \neq 0$ is Ref. 18.
 - [11] J. Jiang, J. Dong, and D. Y. Xing, *Phys. Rev. Lett.* **91**, 056802 (pages 4) (2003).
 - [12] J. Cao, Q. Wang, M. Rolandi, and H. Dai, *Phys. Rev. Lett.* **93**, 216803 (pages 4) (2004).
 - [13] Y. Oreg and A. M. Finkel'stein, *Phys. Rev. Lett.* **74**, 3668 (1995).
 - [14] Another fainter fluctuation with period $\delta V_g \sim 1V$ seems present at $T = 64K$, we are unsure as to its origin.
 - [15] J. Kong, E. Yenilmez, T. W. Tombler, W. Kim, H. Dai, R. B. Laughlin, L. Liu, C. S. Jayanthi, and S. Y. Wu, *Phys. Rev. Lett.* **87**, 106801 (2001).
 - [16] B. L. Altshuler, A. G. Aronov, and D. E. Khmelnitskii, *J. Phys. C* **15**, 7367 (1982).
 - [17] J. von Delft, F. Marquardt, R. A. Smith, and V. Ambegaokar, *cond-mat/0510557*.
 - [18] D. E. Feldman, *Phys. Rev. Lett.* **95**, 177201 (2005).